MADRID
inter.noise 2019
June 16 - 19
NOISE CONTROL FOR A BETTER ENVIRONMENT

Lane-Keeping Control Considering Sensor Noise Based On Improved Artificial Potential Field

Wang Huiran[1], Zhao Linfeng[1+], Jiang Wuhua[1], Tan Dongkui[1], Chen Wuwei[1]

[1]School of Automotive and Transportation Engineering, Hefei University of Technology.
Hefei, 230009, People's Republic of China.

ABSTRACT

To make improvements on lane keeping assistant system (LKAS), the control strategy based on parameter varying artificial potential field (APF) is proposed, which overcomes the shortage that the control precision of traditional APF method could be easily affected by the sensor noise. The reference models of vehicle and the math model of active steering system are established firstly. Then, the parameter varying artificial potential field controller considering vehicle parameter changing (such as vehicle longitudinal and lateral velocities) and sensor noise is designed; the desired steering angle is obtained utilizing the gradient of potential field function. By using trajectory prediction theory, the design parameters of potential field function are determined. The state equation of path tracking error is established to analysis the stability of the lane keeping control system. Finally, the co-simulation based on MATLAB/Simulink and CarSim studies show that the proposed control algorithm not only can assist driver to control vehicle tracking desired lane more accurately but can restrain the sensor noise's disturbance.

Keywords: Artificial potential field, Lane keeping assistant system, Parameter varying
I-INCE Classification of Subject Number:40

1. INTRODUCTION

Among the factors that cause major traffic accidents, the proportion of the driving lane deviation caused by unfocused or mis operation is more and more high. According to statistics, traffic accidents caused by lane deviation account for 30 % of total traffic accidents. In order to ensure the safety of driving and reduce the incidence of major traffic accidents, further research is needed on lane-keeping control system [1].

A large amount of research has been performed on LKAS [2-15]. Enache *et al*. [2] designed an assistant steering controller that prevents vehicle departure from the lane and guarantees driver maneuvering comfort， and an activation strategy for the corresponding assistant intervention was proposed. A hybrid-automata-based lane keeping system model was built by Enache *et al*. [3], and LMI optimization was utilized to solve complex Lyapunov equations and obtain a small overshoot when the vehicle returns to the center line of the lane. The coordination control of the steering and braking systems was adopted by Goodarzi and Ghajar [4], where the ideal steering torque and the ideal yaw torque provided by the braking system by the errors between the vehicle and ideal states were

[1]wanghuiran7@163.com
[2]zhao.lin.feng@163.com

calculated in the upper-layer controller, and the braking torques of each wheel were calculated by the required ideal yaw torque of the braking system.

The limitation of a single-point preview was considered by Jalali *et al*. [5], while a five-point preview method was proposed, in which the preview distance of each point varied with the vehicle speed. The proper weighted values were chosen for the lateral errors of the five points to overcome the limitations of a constant preview distance. Differential braking was adopted by Lee *et al*. [6] for lane keeping, where a layered control model was built. The desired yaw angle velocity preventing vehicle departure from the lane was calculated under the premise of satisfying comfort in the upper-layer controller, and the corresponding braking forces were allocated to each wheel by the desired value in the lower-layer controller. Merah *et al*. [7] proposed a lane keeping auxiliary system based on fuzzy-sliding mode controller. By introducing fuzzy control rules, the auxiliary weights of controller can be changed continuously according to the behavior of the driver. Tan *et al*. [8,9] convert lane departure warning into classification problem, and design a lane departure warning algorithm based on deep neural network. The results show that the proposed lane departure warning algorithm based on deep Fourier neural network can predict lane departure events in a timely manner, and the false alarm rate is significantly reduced compared with the existing method. Saleh *et al*. [10] displays a steering assisted shared control law based on H2 preview control. By integrating the driver model into the vehicle-road model, the driver's behavior is taken into account in the controller design step. Sentouh *et al*. [11] think the driver assistance system should be considered in the ring of the driver in the interference, estimate its intention to minimize the use of intervention controller driver model can realize the balance control precision and coordination.

Distinct from the above mentioned control methods, the artificial potential method, which is extensively applied in solving the path planning of mobile robots to dynamically avoid obstacles, has also been utilized in an LKAS design. The lane-keeping control systems based on the artificial potential method have the advantages of simplicity and ability to operate in real-time and easy combination with the vehicle’s active obstacle avoidance system.

Chen *et al*. [12] proposed a local path planning algorithm for an active obstacle avoidance system for intelligent vehicles based on a repulsive danger force field. An abacus-type repulsive road and danger force field model was built. Consequently, an obstacle avoidance path achieved the required vehicle dynamics performance with the force equilibrium among the road boundary repulsive force, the obstacle boundary repulsive force, and the elastic rope tension. Rossetter *et al*. [13,14] introduced a quadratic potential function for producing a lane-keeping force and designed a Lyapunov function for the vehicle motion and road potential field energies. Their computing method using potential field function parameters guaranteed system stability. A vehicle test was performed on a vehicle equipped with a steer-by-wire system to verify the method’s effectiveness for lane-keeping control and robustness to Improved disturbances.

The abovementioned methods exhibit a good performance in real vehicles. However, the designed potential function only includes vehicle–road direction error information without considering the influences of the vehicle body states. Consequently, the lateral error control precision is not that high. This study introduces two state parameters, namely vehicle longitudinal velocity and vehicle lateral velocity, in the potential field function and proposes a lane-keeping control method based on Improved Artificial Potential Field parameters (IAPFP) to address the problem of low control precision of the artificial potential method in lane-keeping control systems. The lane-keeping steering angle control is then converted to torque control by the Active steering system.

2. SYSTEM METHOD

2.1 System Architecture and Reference Model

2.1.1 Control System Structure

Figure 1 shows the structural framework of the lane-keeping system based on IAPFP. The vehicle longitudinal and lateral velocities and preview error were obtained by the lane-keeping controller to output the desired steering angle. The motor voltage was controlled by the assistant torque controller. The resulting steering angle is used to control vehicles to achieve lane maintenance.

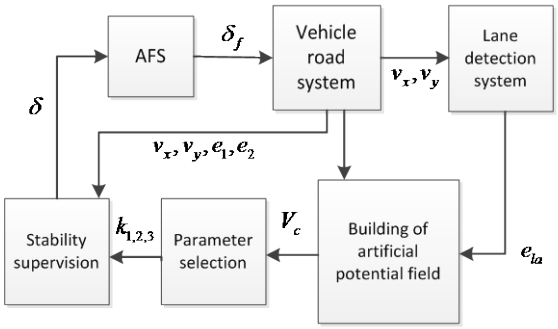

Figure. 1 *Framework of the lane-keeping coordinated control system.*

2.1.2 *Vehicle Model*

The lane-keeping assistant system was generally designed under normal driving conditions, where the vehicle dynamics state was in the linear domain. Therefore, a vehicle model with 2 degrees of freedom could be chosen as the reference model (Figure 2). Its state equations can be expressed as follows [15]:

$$\begin{cases} \dot{v}_y = -\dfrac{a_1}{m v_x} v_y - \left(v_x + \dfrac{a_2}{m v_x} \right) \omega + \dfrac{2C_{\mathrm{f}}}{m} \delta \\ \dot{\omega} = -\dfrac{a_2}{I_z v_x} v_y - \dfrac{a_3}{I_z v_x} \omega + \dfrac{2 l_{\mathrm{f}} C_{\mathrm{f}}}{I_z} \delta \end{cases} \tag{1}$$

where v_x is the vehicle longitudinal velocity; ω is the yaw angle velocity; v_y is the vehicle lateral velocity; δ is the front wheel steering angle; m is the vehicle mass; I_z is the vehicle steering inertia around the vertical axis; C_{f} and C_{r} are the equivalent cornering stiffness for the front and rear tires, respectively; and l_{f} and l_{r} are the distances from the vehicle mass center to the front and rear axles, respectively.

Let α_{f} and α_{r} be the side slip angles for the front and rear tires, respectively, and θ_{f} and θ_{r} be the angles between the velocity directions of the front and rear tires, respectively. The vehicle longitudinal axis is called the velocity angle. Then, $a_1 = 2C_{\mathrm{f}} + 2C_{\mathrm{r}}$, $a_2 = 2C_{\mathrm{f}} l_{\mathrm{f}} - 2C_{\mathrm{r}} l_{\mathrm{r}}$, and $a_3 = 2C_{\mathrm{f}} l_{\mathrm{f}}^2 + 2C_{\mathrm{r}} l_{\mathrm{r}}^2$. The following equations were obtained by adopting a small-angle approximation:

$$\begin{cases} \theta_{\mathrm{f}} = \delta - \alpha_{\mathrm{f}} = \dfrac{v_y + l_f \omega}{v_x} \\ \theta_{\mathrm{r}} = -\alpha_{\mathrm{r}} = \dfrac{v_y - l_f \omega}{v_x} \end{cases} \tag{2}$$

It obtains Eq. (3) from Eqs. (1) and (2):

$$m\left(\dot{v}_y + v_x\omega\right) = -2C_{\mathrm{f}}\theta_{\mathrm{f}} - 2C_{\mathrm{r}}\theta_{\mathrm{r}} + 2C_{\mathrm{f}}\delta \tag{3}$$

From (3), the vehicle lateral force is deemed to be from θ_{f} and θ_{r} .the δ . The control forces produced by the artificial potential field are commonly considered to be equal to the force produced by the front tire's steering angle. The potential field force can then be transferred to the steering angle controlling the vehicle motion.

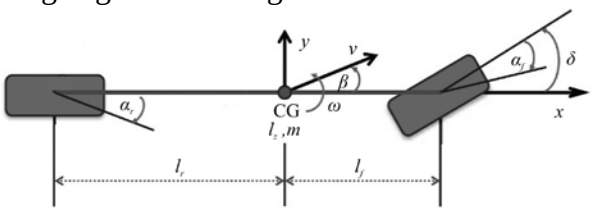

Figure. 2 *Vehicle dynamics model with 2 degrees of freedom.*

2.1.3 Active Steering System *Model*

Figure 3 shows a pillar-type Active steering system that mainly consists of steering wheel assembly, steering executive assembly, a road-feeling motor, a steering motor, a steering angle–steering torque sensor, gear and rack steering gear and an electronic control unit. The active steering system's steering motor is used to produce the LKAS steering torque for overcoming the residence.

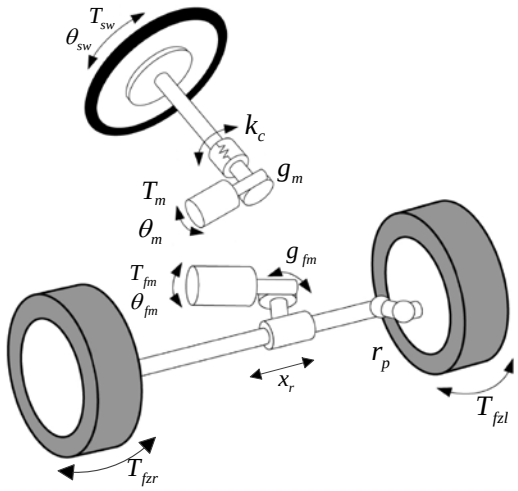

Figure. 3 *Active steering system structure.*

(1) Steering wheel assembly

Steering wheel to torque sensor model as follows:

$$T_{sw} = J_{sw}\ddot{\theta}_{sw} + B_{sw}\dot{\theta}_{sw} + k_c(\theta_{sw} - \theta_m / g_m) + T_{fric} + rand(0, N_t) \tag{4}$$

where θ_{sw} is the steering angle of the steering wheel; θ_m is the steering angle of the motor; g_m is the Speed reduction ratio of road-feeling motor reducer; T_{sw} is the driver torque; T_{fric} is the steering resistance torque of the steering pillar; $rand(0, N_t)$ is random noise and N_t is chosen as 0.3 in this paper ; and J_{sw}, B_{sw} and k_c are the steering inertia, damping, and stiffness of the steering pillar, respectively.

The torque of the motor output axis was obtained as:

$$T_m = J_m\ddot{\theta}_m + B_m\dot{\theta}_m + \frac{k_c(\theta_m / g_m - \theta_{sw})}{g_m} \tag{5}$$

$$T_m = k_t I_a \tag{6}$$

where T_m is the output torque of the motor; I_a is the current of the motor armature; k_t is the torque constant of the motor; and J_m, B_m are the steering inertia and the damping of the motor, respectively.

The electrical equation of the motor was:

$$U_a = R_a I_a + L_a \dot{I}_a + k_e \dot{\theta}_m \tag{7}$$

where U_a is the input voltage of the motor; L_a is the induction coefficient of the motor; and R_a is the internal resistance of the motor.

Steering motor model as follows:

$$T_{fm} = J_{fm}\ddot{\theta}_{fm} + B_{fm}\dot{\theta}_{fm} + \frac{k_{fc}(\theta_{fm} / g_{fm} - x_r / r_p)}{g_{fm}} \tag{8}$$

where θ_{fm} is the steering angle of the steering wheel; g_{fm} is the speed reduction ratio of steering motor reducer; T_{fm} is the driver torque; and J_{fm}, B_{fm} and k_{fc} are the steering inertia, damping, and stiffness of the steering pillar, respectively; x_r is the rack displacement; r_p is the roundness radius of pinion.

The DC motor is used in the steering motor, and its electrical balance equation as follows:

$$U_{fa} = R_{fa} I_{fa} + L_{fa} \dot{I}_{fa} + k_{fe} \dot{\theta}_{fm} \tag{9}$$

$$T_{fm} = k_{ft} I_{fa} \tag{10}$$

where U_{fa} is the input voltage of the motor; L_{fa} is the induction coefficient of the motor; and R_{fa} is the internal resistance of the motor: I_{fa} is the current of the Steering motor.

The gear and rack steering model as follow:

$$M_r \ddot{x}_r + B_r \dot{x}_r + F_{rack} = \frac{k_{fc}(\theta_{fm} / g_{fm} - x_r / r_p)}{r_p} \tag{11}$$

$$F_{rack} = \frac{T_{fzl}}{l_{fl}} + \frac{T_{fzr}}{l_{fr}} \tag{12}$$

where M_r is the quality of gear and rack; B_r is the gear and rack damping coefficient; and F_{rack} is the resistance equivalent to the rack. T_{fzl} and T_{fzr} are the back positive torque of the left front wheel and the right front wheel, respectively; l_{fl} and l_{fr} are the left front wheel and right front wheel steering arm length, respectively.

2.2 Design of the Improved Artificial Potential Field Function Parameters

2.2.1 Design of the Artificial Potential Field Function

The main idea of utilizing the artificial potential field method for the path tracking control is to construct a potential field function representing the vehicle danger degree at different places and perform correction to the state with the lowest danger degree by the

potential force action. The potential field force was determined by the gradient of the potential field function. The derivative of the potential function, which must be continuous, can ensure the smoothness of the control force. In addition, the potential field force should gradually decrease to 0 when the vehicle lateral position approaches the center of the lane to autonomously control the vehicle. Preview information should be included in the potential field function to increase the robustness of the path tracking control for high-speed vehicles. The mathematical expression for the conventional quadratic potential field function is:

$$V_c\left(e_{la}\right)=k\left(e_{la}\right)^2=k\left(e_1+x_{la}\sin e_2\right)^2 \tag{13}$$

where k is the potential field function gain; e_1 is the lateral error to the vehicle mass center; e_{la} is the lateral error at the vehicle preview distance position; e_2 is the error of the vehicle course angle; and x_{la} is the preview distance (Figure 4).

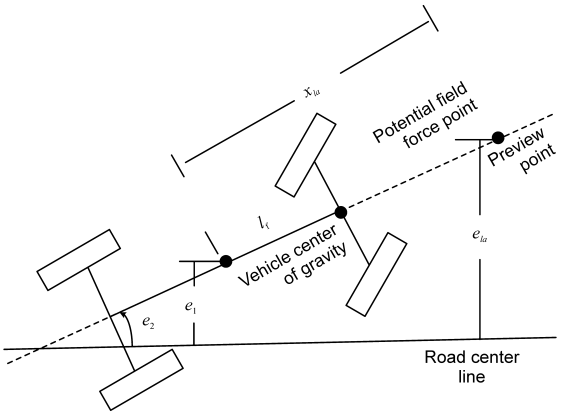

Figure. 4 *Road–vehicle bearing error*

Through Eq. (13), the conventional potential field function simply considered the lateral position error and the directional error between the vehicle and the target path while ignoring the influence of the vehicle dynamics states on the vehicle lateral control. The path tracking control precision was not very high in this case. Thus, two vehicle states (i.e., vehicle longitudinal velocity v_x and lateral velocity v_y) were considered. Accordingly, a preview time t_p was introduced to dynamically adjust the preview distance through the vehicle longitudinal velocity. The new potential field function of the lane-keeping control was obtained as:

$$V_c\left(e_{la}\right)=\left(\frac{k_1}{v_x^2}+k_2\right)\left(e_{la}+k_3v_y\right)^2=\left(\frac{k_1}{v_x^2}+k_2\right)\left(e_1+t_pv_x\sin e_2+k_3v_y\right)^2 \tag{14}$$

Where k_1, $k2$ and k_3 are the design parameters of the potential field function, which required selection with the preview time t_p. The difference of this function from the conventional potential field function was that the function described in Eq. (14) introduced improved parameters v_x and v_y. Thus, the potential field function was dynamically changing. The control force produced by the potential field was usually deemed to act on the vehicle's front axle and equal to the force produced by the front tire's steering angle in Eq. (3). Thus, it obtains:

$$\delta=-\frac{1}{2C_{\mathrm{f}}}\frac{\partial V}{\partial e_{la}}=-\frac{1}{C_{\mathrm{f}}}\left(\frac{k_1}{v_x^2}+k_2\right)\left(e_{la}+k_3v_y\right) \tag{15}$$

2.2.2 Parameter Selection for the Potential Field Function

The four parameters (i.e., k_1, k_2, k_3, and t_p) in Eq. (14) must be determined in advance. The driver preview time t_p was 0.8–1.5 s and selected as $t_p = 1$ s. The preview distance was $x_{la} = v_x$. The lateral error of the vehicle location under the vehicle coordinate system of the current time after t_p was obtained as follows if the cornering angle of the vehicle mass center was $\beta \approx v_y / v_x$ and the steering angle δ was kept constant through the vehicle trajectory predictive formula given by Chen *et al*. [16]:

$$e_V = \tan\left(\frac{G_\omega \delta t_p}{2} + \beta\right) x_{la} \tag{16}$$

where G_ω is the steady-state gain of the vehicle yaw angle velocity to the steering angle.

$$\begin{cases} G_\omega = \dfrac{v_x}{L + K_V v_x^2} \\ K_V = \dfrac{m\left(l_\mathrm{r} C_\mathrm{r} - l_\mathrm{f} C_\mathrm{f}\right)}{2 C_\mathrm{r} C_\mathrm{f} L} \end{cases} \tag{17}$$

where $L = l_\mathrm{f} + l_\mathrm{r}$ is the vehicle axis distance, and K_V is the slope of the vehicle being steered.

The vehicle was expected to move to the target path after the preview time under the control of the steering angle by the potential field force, that is, $e_V = -e_{la}$. A small angle was approximated from Eqs. (1), (15), and (16). It then obtained:

$$\begin{cases} k_1 = 2LC_\mathrm{f} \\ k_2 = 2K_V C_\mathrm{f} \\ k_3 = 1 \end{cases} \tag{18}$$

2.2.3 Stability Analysis of the Closed-Loop System

The state equations of the vehicle lateral position error e_1 and the direction error e_2 were redefined using the vehicle dynamics model in Eq. (1). The following equations can be obtained assuming that the vehicle was driven with a constant longitudinal velocity v_x in a lane of radius R:

$$\begin{cases} \dot{e}_1 = v_y + v_x e_2 \\ e_2 = \psi - \psi_{des} \end{cases} \tag{19}$$

Where ψ_{des} is the lane tangent direction angle. It obtains the state equation model of the tracking error variables [17] as follows by combining Eqs. (1) and (16):

$$\dot{\boldsymbol{x}}_e = \boldsymbol{A}_e \boldsymbol{x}_e + \boldsymbol{B}_{e1}\delta + \boldsymbol{B}_{e2}\dot{\psi}_{des} \tag{20}$$

Where

$$\boldsymbol{x}_e = \begin{pmatrix} e_1 \\ \dot{e}_1 \\ e_2 \\ \dot{e}_2 \end{pmatrix}, \boldsymbol{A}_e = \begin{pmatrix} 0 & 1 & 0 & 0 \\ 0 & \frac{-a_1}{mv_x} & \frac{a_1}{m} & \frac{-a_2}{mv_x} \\ 0 & 0 & 0 & 1 \\ 0 & \frac{-a_2}{I_z v_x} & \frac{a_2}{I_z} & \frac{-a_3}{I_z v_x} \end{pmatrix}, \boldsymbol{B}_{e1} = \begin{pmatrix} 0 \\ \frac{2C_\mathrm{f}}{m} \\ 0 \\ \frac{2C_\mathrm{f} l_\mathrm{f}}{I_z} \end{pmatrix}, \boldsymbol{B}_{e2} = \begin{pmatrix} 0 \\ \frac{-a_2}{mv_x} - v_x \\ 0 \\ \frac{-a_3}{I_z v_x} \end{pmatrix}.$$

The steering angle for the lane-keeping control obtained by combining Eqs. (12), (15), and (16) is:

$$\delta = -2\left(\frac{L}{v_x^2} + K_V\right)\left(e_1 + t_p v_x \sin e_2 + v_y\right) \approx -2\left(\frac{L}{v_x^2} + K_V\right)\left(e_1 + 2v_x e_2 + \dot{e}_1\right) \tag{21}$$

The state equation of the path tracking control for the closed-loop system is then obtained as follows:

$$\dot{\boldsymbol{x}}_e = \boldsymbol{A}_{cl}\boldsymbol{x}_e + \boldsymbol{B}_{e2}\dot{\psi}_{des} \tag{22}$$

where

$$\boldsymbol{A}_{cl} = \begin{pmatrix} 0 & 1 & 0 & 0 \\ b_1 & b_1 - \frac{a_1}{mv_x} & 2b_1 v_x + \frac{a_1}{m} & \frac{-a_2}{mv_x} \\ 0 & 0 & 0 & 1 \\ b_2 & b_2 - \frac{a_2}{I_z v_x} & 2b_2 v_x + \frac{a_2}{I_z} & \frac{-a_3}{I_z v_x} \end{pmatrix},$$

$$b_1 = -\frac{4C_\mathrm{f}}{m}\left(\frac{L}{v_x^2} + K_V\right), b_2 = -\frac{4l_\mathrm{f} C_\mathrm{f}}{I_z}\left(\frac{L}{v_x^2} + K_V\right)$$

The stability of the closed-loop system was determined by the closed-loop matrix $\boldsymbol{A}_{cl}$. $\boldsymbol{A}_{cl}$ only contained one varying parameter v_x, while the trajectory on the S plane of the roots of the characteristic equation of the closed-loop system (i.e., closed-loop poles) was drawn to judge the stability of the closed-loop system when the longitudinal velocity varied in the range of $v_{\min} \le v_x \le v_{\max}$. Figure 5 shows the root locus figure of the closed-loop system when the longitudinal velocity varied from 10 km/h to 120 km/h. All characteristic roots were located in the left half of the plural plane. Therefore, the closed-loop system was stable under the variation of longitudinal velocity within a certain range.

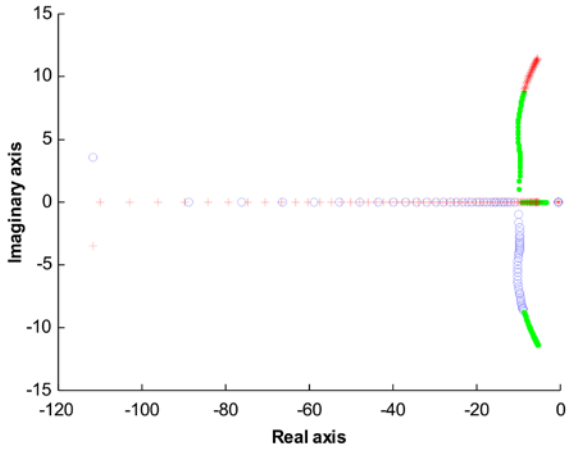

Figure. 5 *Root locus of the closed-loop system while the longitudinal velocity changes.*

3. RESULT

3.1 Simulation Verification

Table 1. Parameters for the vehicle and active steering system models

Quantity	Value
Vehicle mass m/kg	1416
Vehicle moment of inertia about the yaw axis I_z/(kg·m^2)	1770
Distance from the center of mass to the front axle l_f/m	1.02
Distance from the center of mass to the rear axle l_r/m	1.56
Equivalent cornering stiffness of the front wheel C_f/(N/rad)	48701
Equivalent cornering stiffness of the rear wheel C_r/(N/rad)	89690
Steering column moment of inertia J_c/(kg·m^2)	0.046
Steering column damping coefficient B_c(N·m·s/rad)	0.361
Steering column stiffness coefficient K_c/(N·m/rad)	115
Motor moment of inertia J_m/(kg·m^2)	0.00045
Motor damping coefficient B_m/(N·m·s/rad)	0.0033
Motor torque constant K_t/(N·m/A)	0.05
Induction coefficient of motor L_m/H	0.0056
Motor resistance R_m/Ω	0.37
Motor reduction gear ratio N	22
Transmission ratio of the front wheel to the steering column i_{sw}	16.5

In the first simulation driving condition, the LKAS controller individually controlled the vehicle to track the target path; Alt 3 from FHWA in CarSim was chosen as the route; and the road adhesion coefficient was 0.9 (Figure 7). The lane-keeping control results based on the conventional artificial potential field and the proposed IAPFP were compared for the 50, 60, and 80 km/h velocities.

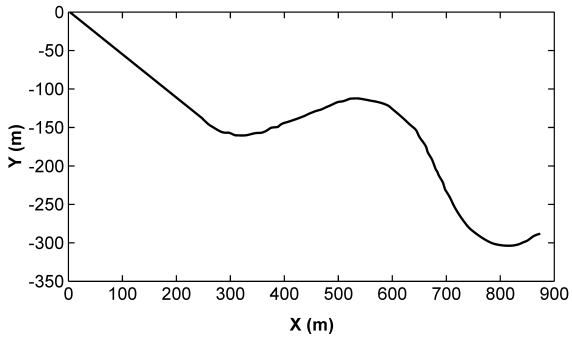

Figure. 6 *Simulation route*

The potential field function parameters of the conventional artificial potential field were determined by the vehicle model for the vehicle longitudinal velocity of 60 km/h. The vehicle lateral errors in Figure 7a can be controlled in a certain range using the two methods. However, the control precision of the conventional artificial potential field was worse on a curved lane. The proposed potential field function considered the vehicle lateral velocity. Meanwhile, the vehicle lateral error control performance was enhanced under the curved lane condition. Compared with that using the conventional method of fixed parameters, a better lane-keeping precision can be obtained using the proposed method of varying potential field function parameters with velocity when the vehicle longitudinal velocity was 50 or 80 km/h.

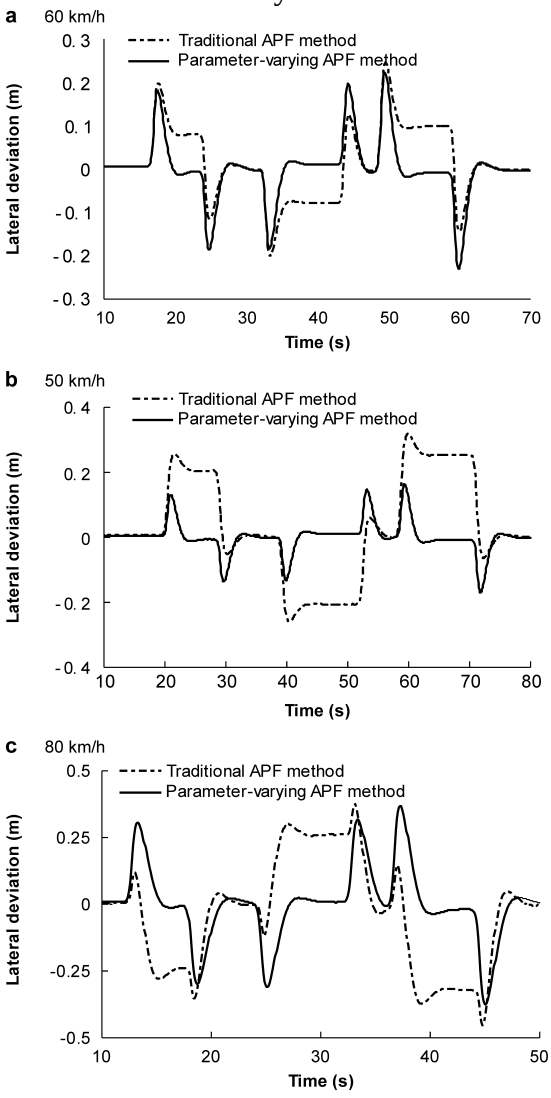

Figure. 7 *Lane-keeping control precision comparison under different velocities.*

In addition, the comparison of the two methods in terms of angle, lateral acceleration and yaw rate are shown in Figure 8. The simulation speed is 80km/h. From Figure 8a, we can see that the controller has less interference on steering wheel angle with the method proposed in the article. Meanwhile, the values of lateral acceleration and yaw rate of vehicle are also smaller than that of traditional APF method. Therefore, the driving stability of vehicles is higher and the occupant will get better travel experience.

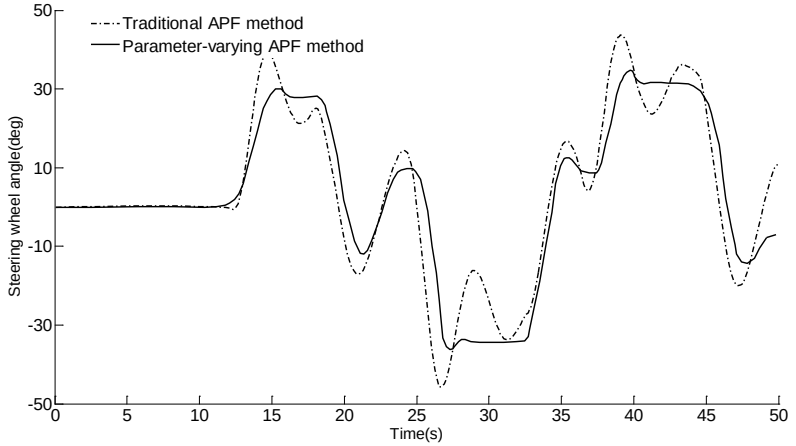

(a)

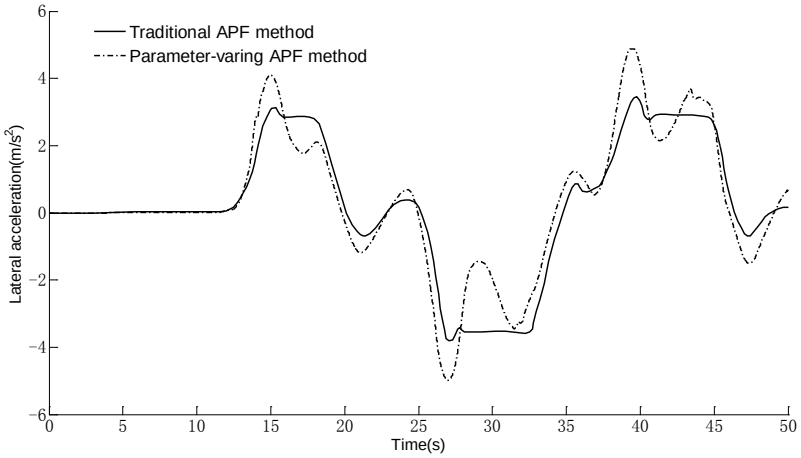

(b)

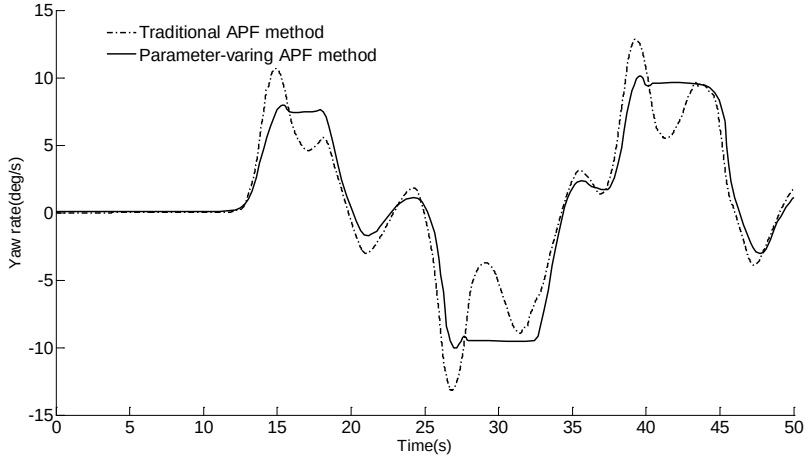

(c)

Fig. 8. *Comparison of control performance between the two methods (80km/h).*

3.2 Hardware-in-Loop Experiment

The proposed method of the Improved Artificial Potential Field parameters was further verified through a hardware-in-loop simulation. Figures 9 show the experimental platform and the equipment framework. The experimental bench consisted of the six following parts: upper-layer computer, lower-layer computer, interface system, steering pillar, active steering system motor controller, and servo motor system used for simulating the steering resistance force. The CarSim full-vehicle dynamics model was built in the upper-layer computer. CarSim and LabVIEW RT were combined to edit the lane-keeping control program. NI PXI was adopted as the lower-layer computer, which runs the simulation program built in the upper-layer computer in real time.

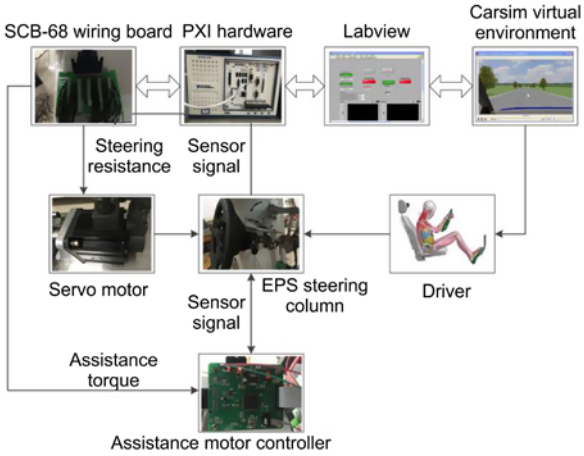

Figure. 9 *Framework of the hardware-in-loop experiment.*

The interface system was responsible for inputting the steering angle. The driver torque was collected by sensors to the PXI real-time control system, while the control signal was output to the actuator's controller (e.g., active steering system motor controller controlling assistant torque and servo motor generating steering road feeling). The vehicle model parameters and the target route in the experiment were the same as those in the simulation.

Figures 10 and 11 illustrate the experimental results of the vehicle lateral error and the steering angle when the driver does not participate in control, and the vehicle longitudinal velocity is 70 km/h. Figure 10 shows that the lane-keeping control precision of the proposed method of the Improved Artificial Potential Field parameters was still better than that of the conventional method. Figure 16 presents the desired and actual steering angles output by the lane-keeping controller, where an error can be observed. A time lag also existed between the actual steering angle and the desired one. This time lag was caused by friction and the motor response's unavoidable relative lag in the real steering system.

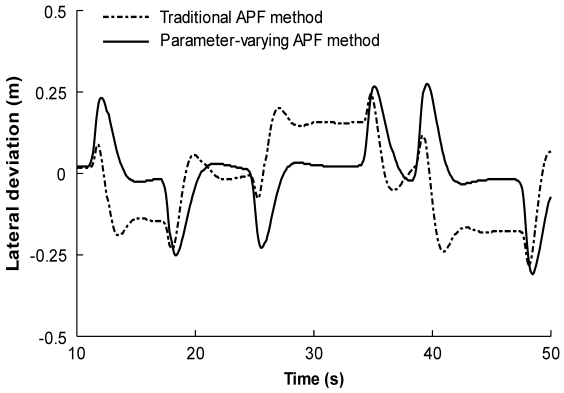

Figure. 10 *Comparison of the vehicle lateral errors.*

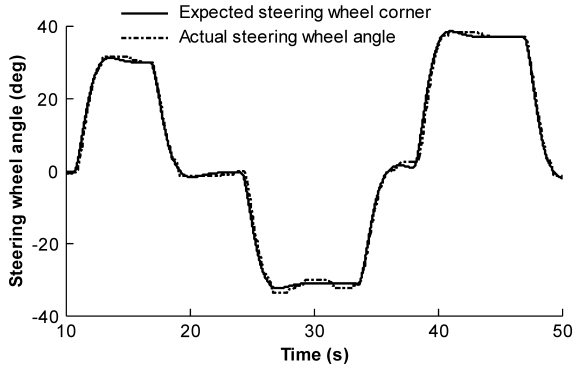

Figure. 11 *Desired and actual steering angles.*

4.CONCLUSIONS

The following conclusions can be drawn from the present study: The influence of the two state parameters, namely vehicle longitudinal velocity and vehicle lateral velocity, on the lane-keeping control was considered.

The method of Improved Artificial Potential Field function parameters was then designed to apply trajectory predictive theory and determine the selection method for the potential field parameters. The path tracking lateral error dynamics model was analyzed. Subsequently, the lane-keeping closed-loop control system was inferred. The stability of the lane-keeping control system based on the Improved Artificial Potential Field parameters was demonstrated by drawing the root locus Figure of the closed-loop system with the change of the vehicle longitudinal velocity.

ACKNOWLEDGEMENTS

The research work was supported under National Nature Science Foundation of China (U1564201, 51675151), Scienceand Technology Major Project in Anhui Province (17030901060).

REFERENCES

1. U. Mellinghoff, T. Breitling, R. Schöneburg, and H.-G. Metzler, “The Mercedes-Benz,” *ATZ worldwide*, vol. 111, no.7–8, pp.34–41, Jul. 2009.
2. N. Minoiu Enache, M. Netto, S. Mammar, and B. Lusetti, “Driver steering assistance for lane departure avoidance,” *Control Eng. Pract.*, vol. 17, no. 6, pp. 642–651, Jun. 2009.
3. N. M. Enache, S. Mammar, M. Netto, and B. Lusetti, “Driver Steering Assistance for Lane-Departure Avoidance Based on Hybrid Automata and Composite Lyapunov Function,” *IEEE Trans. Intell. Transp. Syst.*, vol. 11, no. 1, pp. 28–39, Mar. 2010.
4. A. Goodarzi and M. Ghajar, “Integrating lane-keeping system with direct yaw moment control tasks in a novel driver assistance system,” *Proc. Inst. Mech. Eng. Part K J Multi-body Dyn.*, vol. 229, no. 1, pp. 16–38, Aug. 2014.
5. K. Jalali, S. Lambert, and J. McPhee, “Development of a Path-following and a Speed Control Driver Model for an Electric Vehicle,” *SAE Int. J. Passeng. Cars - Electron. Electr. Syst.*, vol. 5, no. 1, pp. 100–113, Apr. 2012.
6. J. Lee, J. Choi, K. Yi, M. Shin, and B. Ko, “Lane-keeping assistance control algorithm using differential braking to prevent unintended lane departures,” *Control Eng. Pract.*, vol. 23, pp. 1–13, Feb. 2014.

7. A. Merah, K. Hartani, and A. Draou, “A new shared control for lane keeping and road departure prevention,” *Veh. Syst. Dyn.*, vol. 54, no. 1, pp. 86–101, Dec. 2015.
8. D. Tan, W. Chen, J. Wang et al. “Lane departure warning based on deep neural network”[C].// Proceedings of the 17th annual meeting of the China association for science and technology. Hefei University of Technology,2015:1-11.
9. D. Tan, W. Chen and H. Wang, "On the Use of Monte-Carlo Simulation and Deep Fourier Neural Network in Lane Departure Warning," in IEEE Intelligent Transportation Systems Magazine, vol. 9, no. 4, pp. 76-90, winter 2017.
10. L. Saleh, P. Chevrel, F. Claveau, J.-F. Lafay, and F. Mars, “Shared Steering Control Between a Driver and an Automation: Stability in the Presence of Driver Behavior Uncertainty,” *IEEE trans. Intell. Transp. Syst.*, vol. 14, no. 2, pp. 974–983, Jun. 2013.
11. C. Sentouh, S. Debernard, J. C. Popieul, and F. Vanderhaegen, “Toward a Shared Lateral Control Between Driver and Steering Assist Controller,” IFAC Proceedings Volumes, vol. 43, no. 13, pp. 404–409, 2010.
12. Y. Chen, G. Luo, Y. Mei, J. Yu, and X. Su, “UAV path planning using artificial potential field method updated by optimal control theory,” International Journal of Systems Science, vol. 47, no. 6, pp. 1407–1420, Jun. 2014.
13. E. J. Rossetter, J. P. Switkes, and J. C. Gerdes, “Experimental validation of the potential field lane keeping system” *Int. J. Automot. Technol.*, vol. 5, pp. 95–108.
14. E. J. Rossetter and J. C. Gerdes, “Lyapunov Based Performance Guarantees for the Potential Field Lane-keeping Assistance System,” *J. Dyn. Syst. Meas. Control*, vol. 128, no. 3, p. 510–522, 2005.
15. S. Talukdar, M. A. Awan, A. Tremlett, V. Sastry, and D. Purdy, “Preview based Vehicle Steering Control using Neural Networks,” *SAE Technical Papers*, Apr. 2013.
16 . W. Chen, D. Tan, H. Wang, J. Wang, G. Xia, “A Class of Driver Directional Control Model Based on Trajectory Prediction,” *J. Mech. Eng*, vol. 52, no. 14, p. 106, 2016.
17. R. Rajamani, *Vehicle dynamics and control.* NY: Springer, 2011